HHS Public Access

Author manuscript

Adv Mater. Author manuscript; available in PMC 2017 October 01.

Published in final edited form as:

Adv Mater. 2016 October ; 28(37): 8162–8168. doi:10.1002/adma.201601101.

Renal Clearable Organic Nanocarriers for Bioimaging and Drug Delivery

Dr. Homan Kang[‡],
Division of Hematology/Oncology, Department of Medicine, Beth Israel Deaconess Medical Center and Harvard Medical School, Boston, MA 02215 (United States)

Dr. Julien Gravier[‡],
Division of Hematology/Oncology, Department of Medicine, Beth Israel Deaconess Medical Center and Harvard Medical School, Boston, MA 02215 (United States). Institut Albert Bonniot, Université Grenoble Alpes, Grenoble F-38000 (France). INSERM U823, Grenoble F-38000 (France)

Dr. Kai Bao,
Division of Hematology/Oncology, Department of Medicine, Beth Israel Deaconess Medical Center and Harvard Medical School, Boston, MA 02215 (United States)

Dr. Hideyuki Wada,
Division of Hematology/Oncology, Department of Medicine, Beth Israel Deaconess Medical Center and Harvard Medical School, Boston, MA 02215 (United States)

Jeong Heon Lee,
Division of Hematology/Oncology, Department of Medicine, Beth Israel Deaconess Medical Center and Harvard Medical School, Boston, MA 02215 (United States)

Yoonji Baek,
Division of Hematology/Oncology, Department of Medicine, Beth Israel Deaconess Medical Center and Harvard Medical School, Boston, MA 02215 (United States)

GwangLi Park,
Division of Hematology/Oncology, Department of Medicine, Beth Israel Deaconess Medical Center and Harvard Medical School, Boston, MA 02215 (United States)

Prof. Sylvain Gioux,
Division of Hematology/Oncology, Department of Medicine, Beth Israel Deaconess Medical Center and Harvard Medical School, Boston, MA 02215 (United States)

Prof. Brian P. Rubin,

[*]To whom correspondence should be addressed: JLC at jean-luc.coll@ujf-grenoble.fr or HSC at hchoi12@mgh.harvard.edu.
[‡]These authors contributed equally to this work.
Present address:
Dr. H. Kang, Dr. K. Bao, J. H. Lee, Y. Baek, Prof. H. S. Choi, Gordon Center for Medical Imaging, Department of Radiology, Massachusetts General Hospital and Harvard Medical School, Boston, MA 02114 (United States)
Dr. H. Wada, Department of Gastroenterological Surgery II, Hokkaido University Graduate School of Medicine, Sapporo 060-8638 (Japan)
Prof. S. Gioux, ICube Laboratory, University of Strasbourg, Illkirch Cedex F-67412 (France)

Supporting Information is available online from Wiley InterScience or from the author.

Departments of Anatomic Pathology and Cancer Biology, Robert J. Tomsich Pathology and Laboratory Medicine Institute, Lerner Research Institute and Taussig Cancer Center, Cleveland Clinic, Cleveland, OH 44195 (United States)

Prof. Jean-Luc Coll*, and
Institut Albert Bonniot, Université Grenoble Alpes, Grenoble F-38000 (France). INSERM U823, Grenoble F-38000 (France)

Prof. Hak Soo Choi*
Division of Hematology/Oncology, Department of Medicine, Beth Israel Deaconess Medical Center and Harvard Medical School, Boston, MA 02215 (United States)

Graphical Abstract

Renally cleared zwitterionic nanocarriers (H-Dots) are composed of ε-polylysine backbone for charge variations, near-infrared fluorophores for bioimaging, and β-cyclodextrins for potential drug delivery. H-Dots show ideal systemic circulation and rapid distribution and excrete from normal tissue/organ *via* renal excretion after complete targeting to the tumor site without nonspecific uptake by the immune system.

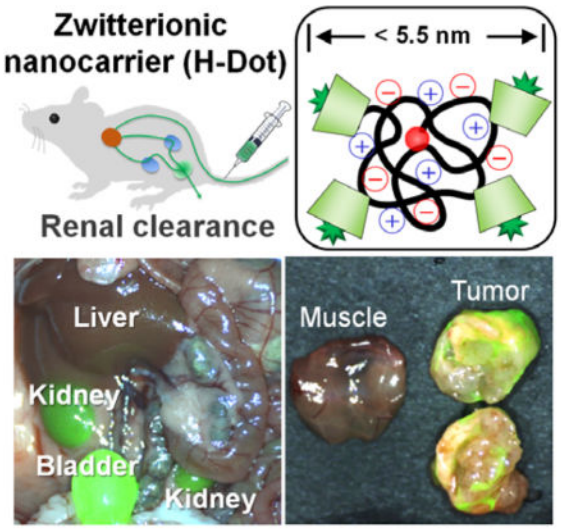

Keywords

Renal clearance; theranostics; optical imaging; nanoparticles; drug delivery

Chemotherapy has led medical oncology along with targeted therapy, radiation therapy, and hormonal therapy.[1] However, standard chemotherapy agents are cytotoxic and often cause serious side effects such as immunosuppression, myelosuppression, mucositis and alopecia due to nonspecific uptake by the immune system and normal cells.[2] Therefore, enormous efforts have been made to develop ideal chemotherapeutic formulations, capable of delivering drugs selectively in cancerous regions without damaging healthy organs.[3]

Recently, theranostic nanocarriers (TNCs) have been developed for disease- and patient-specific diagnosis and treatment.[4,5] TNCs can control the distribution-mediated pharmacokinetics by overcoming several drawbacks of traditional chemotherapeutics including: i) protection of drug from unwanted degradation, ii) prevention of nonspecific interactions, and iii) enhancement of drug absorption into the target tissue.[5] TNCs are composed of inorganic and organic nanomaterials such as silica-based nanoparticles,[6–8] hollow-shells,[9–11] polymer micelles,[12,13] and liposomes[14,15].

The ideal TNC, however, should actively target cancer cells and be safe for normal cells.[16] This generally requires rapid excretion from the body and/or an efficient degradation into nontoxic products.[17] Renal clearance, compared with the hepatobiliary excretion route, is preferred for TNCs because untargeted agents need to be rapidly eliminated from the body with limited cellular internalization/metabolism, thus effectively minimize their exposure to the immune system.[18–20] To this end, it is necessary to understand the key design considerations for TNCs such as hydrodynamic diameter (HD), shape, composition, and surface characteristics based on the “Choi Criteria” that govern the fate of administered TNCs in the body.[17,18,21] Therefore, clinical TNCs should be composed of biocompatible nanomaterials with an overall HD smaller than the threshold of kidney filtration (~5.5 nm) for preferable renal clearance and balanced nonsticky surface charges that can enhance active targeting by reducing nonspecific tissue uptake.[22–24]

Here, we report an ideal TNC (a.k.a. “H-Dot”), composed of biocompatible ε-polylysine (EPL) for various surface modifications, near-infrared (NIR) fluorophores for bioimaging, and β-cyclodextrins (β-CDs) for potential drug delivery (Figure 1a). H-Dots are designed to excrete from normal tissue/organ *via* renal excretion after complete targeting to the tumor site without nonspecific uptake by the immune system. β-CDs (**1**) were conjugated on the primary amine of EPL *via* reductive amination of aldehyde β-CD (Ald-CD; **3**) (**4**) (Figure 1b).[25,26] After purification of resulting CDPLs (**5**) by membrane dialysis, the average number of β-CDs on the EPL backbone was determined to be 6.7 by measuring ^{1}H-NMR (Figure S1). Next, a zwitterionic NIR fluorophore ZW800-1C[27] was conjugated to the terminal amine of CDPL for real-time trafficking after intravenous administration. Once the positively charged ZW800-CDPL (ZW800-CDPL^{+}, **7**) was obtained, the residual amine groups were further modified by using either succinic anhydride (SA) or acetic anhydride (AA), and the number of remaining amine groups was confirmed using ninhydrin test (Figure S2). SA was used to convert the overall charges to be either zwitterionic (ZW800-CDPL$^{\pm}$, **8**) or negative (ZW800-CDPL^{-}, **9**) by reacting with the partial or whole primary amines, respectively (Figure S3). Capping with AA was used to render the CDPL to be non-charged (ZW800-CDPL^{Ac}, **10**). The final physicochemical properties of ZW800-CDPLs with varied charges were summarized in Table S1.

The size exclusion chromatogram of ZW800-CDPL^{+} revealed successful conjugation of ZW800-1C on the polymer backbone with >91% of reaction yield (Figure S4a). The absorbance (solid line) and fluorescence (dotted line) spectra of ZW800-CDPL^{+} (λ_{Abs} = 769 nm; λ_{FL} = 790 nm) represent no spectral changes compared with the control ZW800-1C (Figure S4b).[27] Next, serum stability was confirmed by incubating ZW800-CDPLs with fetal bovine serum (FBS; 5 *w/v*% in saline) at 37 °C (Figure S4c). As a result, the intensities

of absorption and fluorescence decreased slightly over 24 h post-incubation (> 81%), representing the stability of ZW800-CDPLs in the body without optical and physicochemical degradation. The HD of ZW800-CDPLs was calculated by both fluorescence correlation spectroscopy (FCS) and intrinsic viscosity-based approximation. As shown in Table S1, all ZW800-CDPLs were smaller than 5.5 nm, indicating potential and preferable renal clearance.[19]

We then investigated the biodistribution, renal clearance, and pharmacokinetics of four different charged ZW800-CDPLs (+, ±, −, and Ac) in CD-1 mice. The initial distribution was continuously observed for 1 min by the real-time imaging system immediately after a single intravenous injection of each ZW800-CDPL. Overall, ZW800-CDPLs distributed rapidly in the blood, heart, lung, liver, and other major organs within 1 min post-injection, and then gradually accumulated into kidneys, followed by renal excretion to the bladder. The NIR fluorescence signals of ZW800-CDPLs were mainly located in the urinary system 4 h post-injection (Figure 2a). Interestingly, ZW800-CDPL^{+} showed relatively high fluorescence in liver and abdominal cavity because of electrostatic interactions with negatively charged cell membrane.[28] In contrast, all the other ZW800-CDPLs left no fluorescence signals in the liver, of which signal-to-background ratio (SBR; organs *vs.* muscle) was calculated in Figure 2b,c along with other resected organs. These results indicate that zwitterionic, negative, or acetylated CDPLs can elude nonspecific uptake by the reticuloendothelial system (RES) and exclusively excrete (>80 %ID) to the bladder within 4 h post-injection (Figure 2d).

As shown in Table S2, the pharmacokinetic parameters of ZW800-CDPLs were summarized after a single intravenous injection. The blood concentration curves represent that ZW800-CDPLs exhibit a two-compartment profile of *in vivo* kinetics (Figure 3a). The rapid initial decay of blood concentration was reflected by the efficient initial distribution into capillaries, and the final concentrations after 4 h post-injection reached close to 0 %ID/g representing rapid elimination from the body by the systemic clearance. The half-life values of ZW800-CDPLs (Figure 3b) are ranging from 0.52±0.12 (ZW800-CDPL^{-}) to 2.86±0.15 min (ZW800-CDPL^{+}) during the distribution phase ($t_{1/2\alpha}$), and from 14.41±1.25 (ZW800-CDPL^{Ac}) to 39.80±4.17 (ZW800-CDPL^{+}) for the terminal phase ($t_{1/2\beta}$). Among them, ZW800-CDPL^{+} showed relatively longer blood half-lives than the other ZW800-CDPLs (**P <0.01), which might be resulted from the nonspecific interaction associated with plasma proteins. In addition, urinary excretion of non-positive charged ZW800-CDPLs was >80 %ID at 4 h post-injection (Figure 3c), while only approximately 45 %ID of ZW800-CDPL^{+} was found in the bladder (**P <0.01). The blood clearance and urinary excretion of CDPLs are similar to those of renal clearable small molecule fluorophores such as ZW800-1,[29] ZW800-1C,[27] and ZW700-1,[30] but much faster than those of previously reported renal clearable inorganic nanoparticles such as silica,[20] gold cluster,[31] and quantum dots[17,18,21]. The values for plasma clearance and volume of distribution were estimated based on the pharmacokinetics data depicted in Figure 3d. Despite the relatively short blood half-life, the plasma clearance value of zwitterionic ZW800-CDPL appeared to be 0.21 mL/min, which is 2.6-fold faster than that of negative or acetylated CDPLs. Interestingly, the volume of distribution for ZW800-CDPL$^{\pm}$ also showed the highest value among the tested albeit no significant signals in the major organs except kidneys. To support

these results, protein binding assay was carried out by incubating ZW800-CDPLs in 5% FBS for 4 h, and gel filtration chromatography (GFC) was used to measure the changes in retention time. Consequently, the zwitterionic CDPL exhibited only minimum adsorption with serum proteins (14%), while charged CDPL^{+} and CDPL^{-} resulted in 23% and 26% of protein binding, respectively (Table S1). This is well explained by the pharmacokinetics data including plasma clearance and volume of distribution for CDPL derivatives: ZW800-CDPL$^{\pm}$ systemically circulated and distributed to the whole body without nonspecific uptake by the RES, then eliminated efficiently from the body.

To demonstrate efficient tumor targeting and drug delivery using zwitterionic CDPL, we additionally recruited both xenograft and genetically engineered gastrointestinal stromal tumor (GIST) mouse models.[32] Imatinib, a tyrosine-kinase inhibitor for treating GIST, was selected as a therapeutic drug because it forms a 1:1 stoichiometric host-guest complex with β-CD.[33] Imatinib was conjugated with a fluorescent dye, Cy3 NHS Ester (GE Healthcare), to track the distribution and clearance of imatinib in tumor-bearing mice (Figure S6a). Prior to carrying out *in vivo* tumor targeting, the imatinib- CDPL$^{\pm}$ inclusion complex was tested for pH-induced drug release by measuring the changes in absorbance spectra of Cy3 (Figure S6b,c). While imatinib-loaded ZW800-CDPL$^{\pm}$ was relatively stable at pH 7.4, up to 60% of imatinib was released from the CDPL delivery vehicle in 12 h post-incubation at pH 5.0 due to the reduced hydrophobic interactions between imatinib and the apolar cavity of β-CD. This result suggests that the inclusion complex is stable at the physiological environment (pH 7.4), but releases the complexed drugs efficiently in the tumor microenvironment (pH 5.0).

Next, the imatinib-CDPL$^{\pm}$ complex was administered intravenously into GIST-bearing xenograft mice, and real-time intraoperative NIR imaging was performed for 24 h post-injection (Figures 4a and S7). The tumor-to-background ratio (TBR) increased significantly over the time course of 12 h post-injection, and remained constant up to 24 h. This result demonstrates that the imatinib-loaded CDPL$^{\pm}$ successfully target the tumor region by the enhanced permeation and retention (EPR) effect. We then sacrificed the xenograft mice at 24 h post-injection and observed their abdominal cavity to confirm biodistribution and clearance (Figure 4b). Almost no background signal was observed in the major organs except the urinary excretory system including kidneys and bladder where ZW800-CDPL$^{\pm}$ is actively being eliminated. Tumors were resected subsequently along with other tissues and organs, and their NIR fluorescence signal was compared against to muscle, of which TBR marked over 8.0 (Figure 4b).

Furthermore, the drug delivery and tumor targeting efficiency of zwitterionic CDPL was demonstrated in genetically engineered GIST mice having tumors in the cecum area since birth.[32] The imatinib-CDPL$^{\pm}$ complex was injected intravenously into the GIST-bearing mice 24 h prior to imaging, and their tumors were imaged along with duodenum, intestine, and muscle (Figure 4c). The complex successfully targeted tumors around the cecum, but showed partial uptake in liver and pancreas. This is mainly because of the lipophilicity of imatinib, which is not fully compensated by the formation of inclusion complex with β-CD as well as by the zwitterionic property of CDPL (Figure S7c). However, it cannot be overstated that the imatinib-loaded CDPL could avoid nonspecific uptake by lung and

spleen, while the same dose of imatinib-conjugated with ZW800-1 showed relatively high nonspecific uptake by the RES because of interaction with macrophages (data not shown). Tumors were then resected, and the intratumoral microdistribution of imatinib-loaded CDPL$^{\pm}$ was investigated by H&E histology and fluorescence microscopy (Figure 4d). Fluorescence images by red (590–650 nm) and NIR (790–830 nm) filters were taken in order to detect Cy3-imatinib and ZW800-CDPL, respectively. Interestingly, ZW800-CDPL$^{\pm}$ (pseudocolored in lime green) was predominantly observed in the boundary of tumoral regions and the signals of Cy3-imatinib (pseudocolored in red) were spread out intratumorally. This result indicates that zwitterionic CDPLs can successfully deliver hydrophobic drugs to the tumor site by forming a stable inclusion complex, and the anticancer drug is released from the delivery vehicle at the acidic pH generated by the tumor microenvironment.

In conclusion, we designed an innovative nanocarrier (a.k.a. H-Dot) that delivers anticancer drugs to the tumors without trapping into the immune system, followed by the rapid renal clearance of untargeted agents from the body. H-Dots allow early detection of target tumor due to rapid distribution and fast clearance, which drastically reduce nonspecific background uptake, thus, enhance target-to-background ratio. These nanocarriers are composed of biocompatible EPL and β-CD for delivering drugs and/or contrast agents to the target, and their global electric charges can be controlled from negative to neutral or positive. Among the tested 4 different ZW800-CDPL derivatives, zwitterionic CDPL is of particular interest since it presents 1) rapid systemic circulation and whole body distribution, 2) the lowest nonspecific capture by the RES, and 3) complete excretion to the bladder within 24 h. These precisely designed H-Dots could be used as a promising theranostic nanoplatform that potentially reduce the side effects of conventional chemotherapies when combined with appropriate anticancer drugs.

Experimental Section

Synthesis of ZW800-CDPL

To form the *N*-hydroxysuccinimide (NHS)-activated ester, ZW800-1C[27,30] (500 mg, 0.5 mmol) was dissolved in 50 mL of anhydrous DMSO. Then, 0.5 mL of *N,N*-diisopropylethylamine (DIEA) and dipyrrolidino(N-succinimidyloxy)carbenium hexafluorophosphate (HSPyU; 410 mg, 1 mmol) were added to the solution. After stirring for 2 h at room temperature, the reaction mixture was poured in 250 mL of acetone/ethanol (1:1 *v/v*). The precipitate was filtered and washed with acetone/ethanol several times to remove excess reagents. The resulting ZW800-1C NHS ester was dried overnight *in vacuo*. For conjugation, ZW800-1C-NHS ester (50 μmol) was added to CDPL (400 mg, 25 μmol) in 5 mL of PBS (pH 8.0). The reaction mixture was stirred for 12 h, then excess reagents were removed by Vivaspin centrifugal filters (10 kDa MWCO; Sartorious, New York, NY). The resulting filtrate was lyophilized to yield the desired ZW800-CDPL product.

Charge variations of ZW800-CDPLs

To obtain various charged ZW800-CDPLs, predetermined amounts of succinic anhydride (SA; 3 μmol for CDPL$^{\pm}$, and 20 μmol for CDPL^{-}) or acetic anhydride (AA; 20 μmol for

$CDPL^{Ac}$) were added into each ZW800-$CDPL^{+}$ in PBS (pH 8.0; 1 μmol in 0.5 mL), and the mixture was vortexed for 1.5 h at room temperature. The solution was precipitated by adding acetone (14 mL) and washed with acetone five times followed by centrifugation to remove excess reagents (see Supplementary Methods for details).

In vivo tumor targeting and drug delivery

Animals were housed in an AAALAC-certified facility and were studied under the supervision of BIDMC IACUC in accordance with the approved institutional protocol (# 057-2014). To establish tumor-xenografted nude mice, GIST cell was cultured in DMEM with 5% FBS and 100 units/ml of penicillin and streptomycin. NCr nu/nu mice (Taconic Farms, Germantown, NY) were inoculated subcutaneous injection with 2×10^6 GIST cells suspended in 150 μL of saline/matrigel (50 *v/v*%) at the left flank. Once the tumor reached a size of 0.5 cm, 40 nmol of Cy3-loaded ZW800-$CDPL^{\pm}$ in saline containing 5% BSA was injected through tail vein. Tumor mice were imaged using our real-time intraoperative NIR imaging system at the following time points (10, 30, 60, 120, 180, 240, 720 and 1440 min) and then scarified for *ex vivo* imaging and histological evaluations. For histology, fluorescence microscopy was performed on a Nikon TE2000 with two custom filter sets (Chroma Technology, Brattleboro, VT, USA).

Quantitative analysis

The fluorescence and background intensities of a region of interest over each tissue were quantified using customized imaging software and ImageJ v1.48 (National Institutes of Health, Bethesda, MD). The signal-to-background ratio (SBR) was calculated as SBR = fluorescence/background, where background is the fluorescence intensity of muscle. A one-way *ANOVA* followed by Tukey's multiple comparisons test was used to assess the statistical difference. *P* value of less than 0.05 was considered significant: $*P<0.05$, $**P<0.01$, and $***P<0.001$. Results are presented as mean ± standard deviation (s.d.).

Supplementary Material

Refer to Web version on PubMed Central for supplementary material.

Acknowledgments

This study was supported by the following grants: European Project FP7 PIOF-GA-2011-303069 NanoPDT, NIH/NIBIB grant #R01-EB-011523, and Basic Science Research Program through the NRF of Korea (NRF-2014-R1A6A3A03057790).

References

1. Gadducci A, Cosio S, Genazzani AR. Crit Rev Oncol Hematol. 2006; 58:242–256. [PubMed: 16436330]
2. Chari RV. Adv Drug Delivery Rev. 1998; 31:89–104.
3. Müller R, Jacobs C, Kayser O. Adv Drug Delivery Rev. 2001; 47:3–19.
4. Li Y, Lin T-y, Luo Y, Liu Q, Xiao W, Guo W, Lac D, Zhang H, Feng C, Wachsmann-Hogiu S, Walton JH, Cherry SR, Rowland DJ, Kukis D, Pan C, Lam KS. Nat Commun. 2014; 5:4712. [PubMed: 25158161]

5. Peer D, Karp JM, Hong S, Farokhzad OC, Margalit R, Langer R. Nat Nanotechnol. 2007; 2:751–760. [PubMed: 18654426]
6. Lee JE, Lee N, Kim T, Kim J, Hyeon T. Acc Chem Res. 2011; 44:893–902. [PubMed: 21848274]
7. Ambrogio MW, Thomas CR, Zhao YL, Zink JI, Stoddart JF. Acc Chem Res. 2011; 44:903–913. [PubMed: 21675720]
8. Singh N, Karambelkar A, Gu L, Lin K, Miller JS, Chen CS, Sailor MJ, Bhatia SN. J Am Chem Soc. 2011; 133:19582–19585. [PubMed: 21981330]
9. Noh MS, Lee S, Kang H, Yang JK, Lee H, Hwang D, Lee JW, Jeong S, Jang Y, Jun BH, Jeong DH, Kim SK, Lee YS, Cho MH. Biomaterials. 2015; 45:81–92. [PubMed: 25662498]
10. Jang H, Kim YK, Huh H, Min DH. ACS Nano. 2014; 8:467–475. [PubMed: 24383549]
11. You J, Zhang G, Li C. ACS Nano. 2010; 4:1033–1041. [PubMed: 20121065]
12. Chung JE, Tan S, Gao SJ, Yongvongsoontorn N, Kim SH, Lee JH, Choi HS, Yano H, Zhuo L, Kurisawa M, Ying JY. Nature Nanotechnology. 2014; 9:907–912.
13. Hirsjarvi S, Dufort S, Gravier J, Texier I, Yan Q, Bibette J, Sancey L, Josserand V, Passirani C, Benoit JP, Coll JL. Nanomedicine. 2013; 9:375–387. [PubMed: 22960195]
14. Al-Jamal WT, Kostarelos K. Acc Chem Res. 2011; 44:1094–1104. [PubMed: 21812415]
15. Torchilin VP. Nat Rev Drug Discovery. 2005; 4:145–160. [PubMed: 15688077]
16. Chen F, Ehlerding EB, Cai W. J Nucl Med. 2014; 55:1919–1922. [PubMed: 25413134]
17. Choi HS, Frangioni JV. Mol Imaging. 2010; 9:291–310. [PubMed: 21084027]
18. Kang H, Mintri S, Menon AV, Lee HY, Choi HS, Kim J. Nanoscale. 2015; 7:18848–18862. [PubMed: 26528835]
19. Choi HS, Liu W, Misra P, Tanaka E, Zimmer JP, Itty Ipe B, Bawendi MG, Frangioni JV. Nat Biotechnol. 2007; 25:1165–1170. [PubMed: 17891134]
20. Phillips E, Penate-Medina O, Zanzonico PB, Carvajal RD, Mohan P, Ye Y, Humm J, Gonen M, Kalaigian H, Schoder H, Strauss HW, Larson SM, Wiesner U, Bradbury MS. Sci Transl Med. 2014; 6:260ra149.
21. Choi HS, Liu W, Liu F, Nasr K, Misra P, Bawendi MG, Frangioni JV. Nat Nanotechnol. 2010; 5:42–47. [PubMed: 19893516]
22. Choi HS, Liu W, Misra P, Tanaka E, Zimmer JP, Itty Ipe B, Bawendi MG, Frangioni JV. Nat Biotechnol. 2007; 25:1165–1170. [PubMed: 17891134]
23. Longmire M, Choyke PL, Kobayashi H. Nanomedicine. 2008; 3:703–717. [PubMed: 18817471]
24. Yu M, Zheng J. ACS Nano. 2015; 9:6655–6674. [PubMed: 26149184]
25. Choi HS, Yamashita A, Ooya T, Yui N, Akita H, Kogure K, Ito R, Harashima H. Chembiochem. 2005; 6:1986–1990. [PubMed: 16222730]
26. Choi HS, Huh KM, Ooya T, Yui N. J Am Chem Soc. 2003; 125:6350–6351. [PubMed: 12785758]
27. Hyun H, Owens EA, Narayana L, Wada H, Gravier J, Bao K, Frangioni JV, Choi HS, Henary M. RSC Adv. 2014; 4:58762–58768. [PubMed: 25530846]
28. Salatin S, Maleki Dizaj S, Yari Khosroushahi A. Cell Biol Int. 2015; 39:881–890. [PubMed: 25790433]
29. Choi HS, Nasr K, Alyabyev S, Feith D, Lee JH, Kim SH, Ashitate Y, Hyun H, Patonay G, Strekowski L, Henary M, Frangioni JV. Angew Chem Int Ed. 2011; 50:6258–6263.
30. Hyun H, Henary M, Gao T, Narayana L, Owens EA, Lee JH, Park G, Wada H, Ashitate Y, Frangioni JV, Choi HS. Mol Imaging Biol. 2015:1–10. [PubMed: 25238997]
31. Liu J, Yu M, Zhou C, Yang S, Ning X, Zheng J. J Am Chem Soc. 2013; 135:4978–4981. [PubMed: 23506476]
32. Rubin BP, Fletcher JA, Fletcher CD. Int J Surg Pathol. 2000; 8:5–10. [PubMed: 11493959]
33. Beni S, Szakacs Z, Csernak O, Barcza L, Noszal B. Eur J Pharm Sci. 2007; 30:167–174. [PubMed: 17145172]

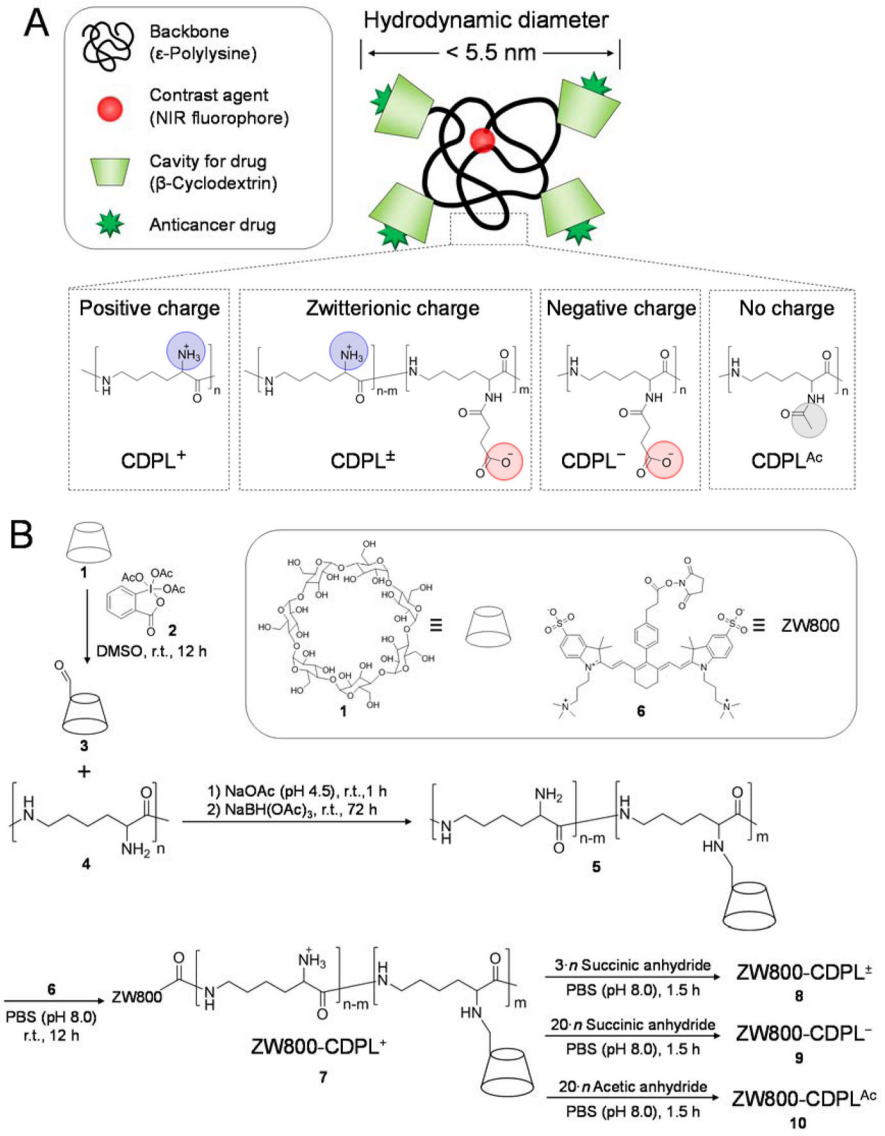

Figure 1.

Schematic diagrams of CDPL-based TNCs for drug delivery. (A) CDPL-based nanocarriers and charge variations including positive (+), zwitterionic (±), negative (−), and no charges (Ac). (B) Synthetic scheme of charge varied CDPLs conjugated with ZW800-1C.

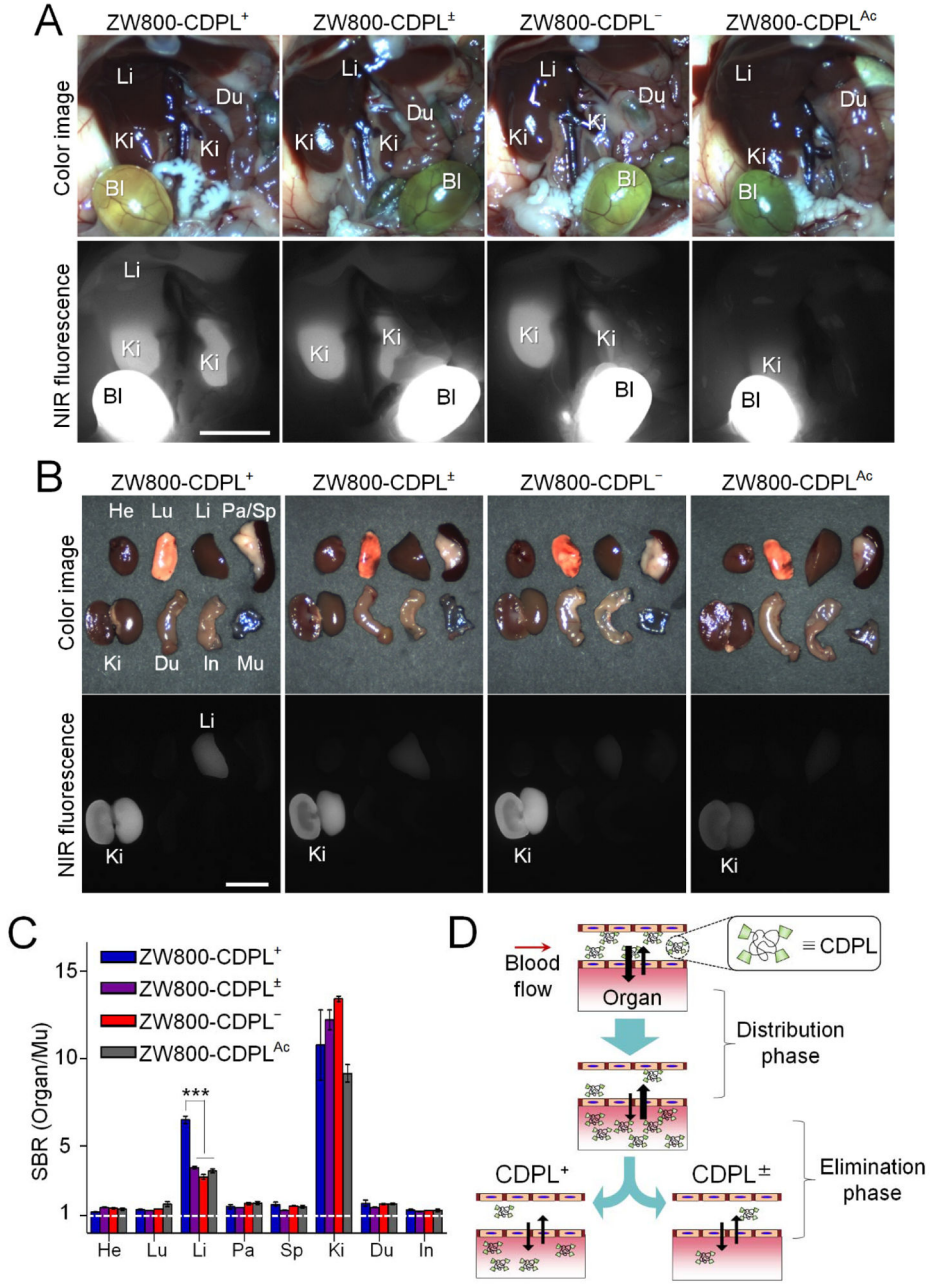

Figure 2.

In vivo biodistribution of various charged ZW800-CDPLs. Each ZW800-CDPL (10 nmol) was injected intravenously into CD-1 mice, and their NIR fluorescence images of (A) abdominal cavity and (B) resected organs 4 h post-injection. (C) SBR of each organ against muscle (Mu). Abbreviations used are: Bl, bladder; Du, duodenum; He, heart; In, intestine; Ki, kidneys; Li, liver; Lu, lungs; Mu, muscle; Pa, pancreas; Sp, spleen. Exposure time, 25 ms; scale bar, 1 cm (n = 3, mean ± s.d., ***P<0.001).

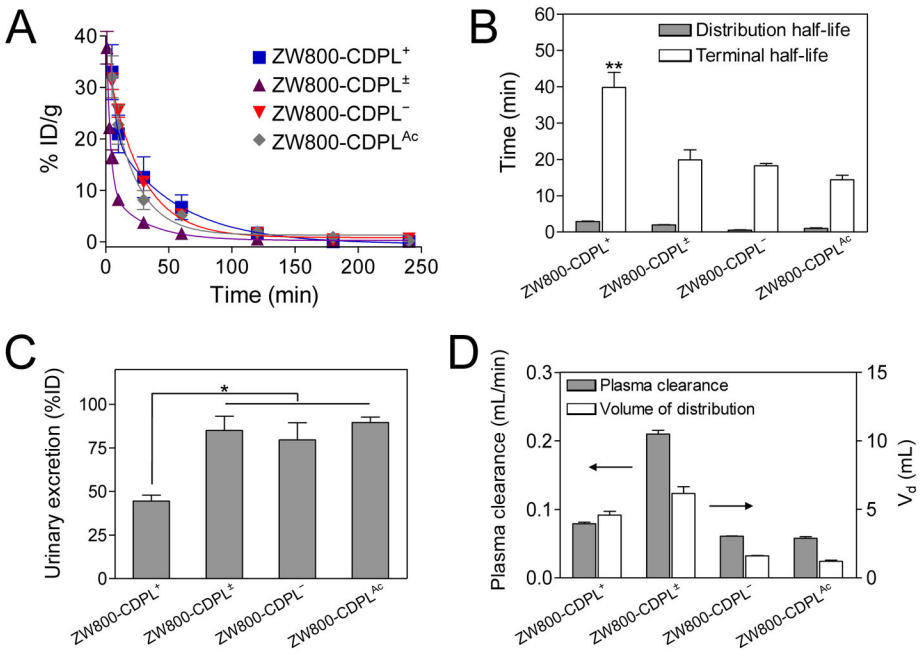

Figure 3.

Pharmacokinetics of positive, zwitterionic, negative, and acetylated CDPLs. 10 nmol of each ZW800-CDPL was injected intravenously into CD-1 mice, and their (A) blood concentration (%ID/g) decay, (B) distribution and elimination half-life, (C) urinary excretion, and (D) plasma clearance and volume of distribution (V_d) were observed for 4 h post-injection (n = 3, mean ± s.d., *P <0.05 and **P <0.01).

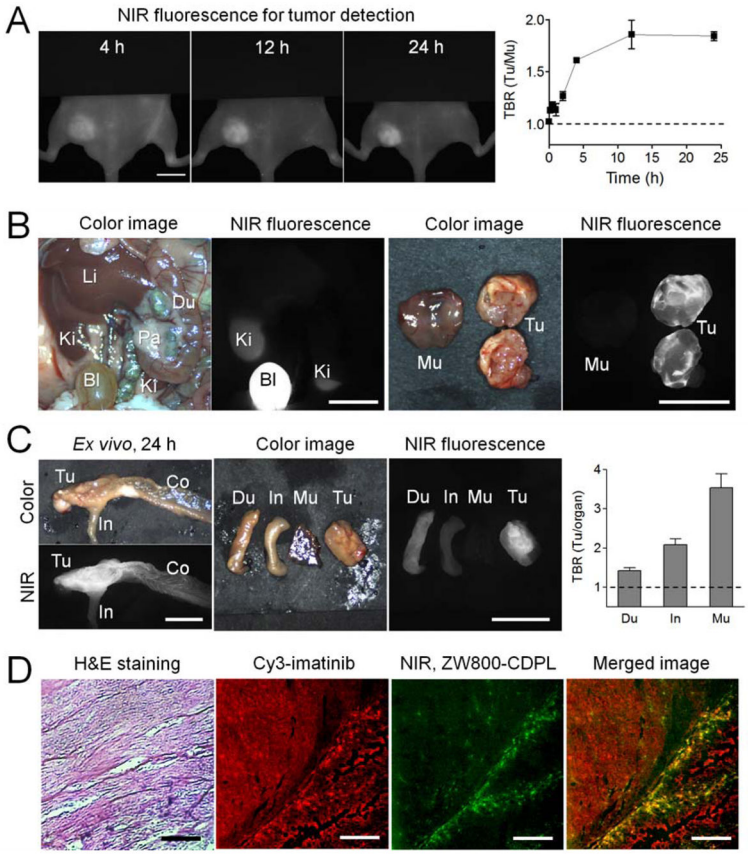

Figure 4.

Tumor targeting and drug delivery of zwitterionic CDPL by forming an inclusion complex with imatinib. (A) Cy3-imatinib loaded ZW800-CDPL$^{\pm}$ (40 nmol) was injected intravenously into xenograft GIST-bearing mice, and the TBR (tumor/muscle) was measured for 24 h post-injection. (B) *In vivo* and *ex vivo* NIR fluorescence imaging of xenograft mice shown in (A) at 24 h post-injection. Abbreviations used are: Du, duodenum; Mu, muscle; Li, liver; Ki, kidney; Pa, pancreas Tu, tumor. Scale bars, 1 cm. (C) 40 nmol of Cy3-imatinib loaded ZW800-CDPL$^{\pm}$ was injected intravenously into genetically engineered GIST mice, and their *ex vivo* NIR fluorescence images were obtained at 24 h post-injection. TBR was measured against duodenum (Du), intestine (In), and muscle (Mu), respectively. Abbreviations used are: Co, colon; Tu, tumor. Scale bars, 1 cm. (D) Histopathological analysis of resected tumor from genetically engineered GIST-bearing mice. Shown are H&E staining, Cy3-labeld imatinib (pseudocolored in red), ZW800-CDPL$^{\pm}$ (pseudocolored in lime green), and merged image of the two. Sale bars, 100 μm.